

A fully-coupled computational framework for large-scale simulation of fluid-driven fracture propagation on parallel computers

Bianca Giovanardi^a, Santiago Serebrinsky^b, Raúl Radovitzky^{a,*}

^a*Massachusetts Institute of Technology,
77 Massachusetts Ave, Cambridge, MA 02139, U.S.A.*

^b*Y-TEC, YPF Tecnología, S.A.
Calle Baradero, Ensenada, 1925, Buenos Aires, Argentina*

Abstract

The propagation of cracks driven by a pressurized fluid emerges in several areas of engineering, including structural, geotechnical, and petroleum engineering. In this paper, we present a robust numerical framework to simulate fluid-driven fracture propagation that addresses the challenges emerging in the simulation of this complex coupled nonlinear hydro-mechanical response. We observe that the numerical difficulties stem from the strong nonlinearities present in the fluid equations as well as those associated with crack propagation, from the quasi-static nature of the problem, and from the *a priori* unknown and potentially intricate crack geometries that may arise. An additional challenge is the need for large scale simulation owing to the mesh resolution requirements and the expected 3D character of the problem in practical applications. To address these challenges we model crack propagation with a high-order hybrid discontinuous Galerkin / cohesive zone model framework, which has proven massive scalability properties, and we model the lubrication flow inside the propagating cracks using continuous finite elements, furnishing a fully-coupled discretization of the solid and fluid equations. We find that a conventional Newton-Raphson solution algorithm is robust even in the presence of crack propagation. The parallel ap-

*Corresponding author
Email address: rapa@mit.edu (Raúl Radovitzky)

proach for solving the linearized coupled problem consists of standard iterative solvers based on domain decomposition. The resulting computational approach provides the ability to conduct highly-resolved and quasi-static simulations of fluid-driven fracture propagation with unspecified crack path. We conduct a series of numerical tests to verify the computational framework against known analytical solutions in the toughness and viscosity dominated regimes and we demonstrate its performance in terms of robustness and parallel scalability, enabling simulations of several million degrees of freedom on hundreds of processors.

Keywords: Fluid-driven fracture propagation, Discontinuous Galerkin finite elements, cohesive zone model, crack propagation with unspecified path, massive parallel scalability

1. Introduction

Fluid-driven fracture propagation concerns several areas of engineering, including structural, geotechnical, and petroleum engineering. In recent times there has been a flourishing of research geared at delivering computational tools for simulating fluid-driven fracture propagation, mostly driven by the oil industry, where numerical simulations can be used to support the design of field operations by providing a physics-based framework to complement legacy approaches based on accumulated experience and statistical inference, therefore helping reduce economic risk. The interested reader can consult, for example, [1] for a recent review of numerical methods that have been proposed to tackle this problem.

A thorough mathematical description of the complex physical problem associated with the injection of pressurized fluid in a deformable solid requires the consideration of several coupling mechanisms among the fluid flow, the deformation of the solid material and the possible propagation of cracks as a result of material failure [2]. The injection of fluid results in a pressure applied on the crack walls. Material deformation and crack propagation increase the volume

available to the fluid and therefore affect the pressure distribution as well as the fluid flow. A basic mathematical model for this problem involves the elastostatics equations which govern the deformation and stress field in the solid, the equations for the fluid flow inside the cracks, and a proper model for describing crack propagation, which mathematically renders the problem of the moving boundary type. Depending on the specific application, additional refinements of the model may include the consideration of leakage of fluid off the fracture walls into the adjacent porous rock, the transport of proppant and the chemical reactions involved, and the effects of temperature on the rheology of the injected fluids.

Early analytical progress in the description of fluid-driven fracture propagation was made by Khristianovic, Geertsma and de Klerk [3, 4], who devised a one dimensional analytical model for a plane-strain straight crack whose propagation is driven by the injection of an incompressible viscous fluid at a constant rate. This model, referred to as KGD, solves the coupled equations of elastostatics for the solid, lubrication flow and mass conservation for the fluid. Further systematic studies by Detournay *et al.* have provided a complete picture of the simplified and analytically-tractable one-dimensional problem [5, 6, 7, 8, 9, 10]. Specific advances included the identification and classification of asymptotic regimes where analytical solutions were found, each presenting unique characteristics in terms of near tip asymptotic behavior, including the possible occurrence of boundary layers in certain regimes.

It is well-established that computational models can complement and significantly expand the extent of the analyses available to analytical methods by providing a full-field, albeit discretized, description of the problem of interest. In the case of fluid-driven fracture propagation, the coupled elasto-hydrodynamics problem is typically discretized using the finite element method to solve the elastic problem [11, 12, 13], while finite differences [11], finite elements [12], or finite volumes [13] have been employed for modeling the lower dimensional fluid flow. It bears emphasis that even in the absence of crack propagation the hydro-mechanical coupling is extremely strong, since the ability of the fluid to

flow in the fracture depends nonlinearly on the fracture opening.

Different numerical strategies have been proposed to describe fracture propagation in the solid and to evolve the fluid computational domain as cracks propagate. A recent review paper [1] has described these approaches, identifying their main advantages and limitations.

Cohesive zone models (CZM) have been widely used for their sound fracture mechanics basis and their ease of implementation as interface elements within finite element frameworks. In the context of fluid-driven fracture propagation, the effectiveness of this approach has been verified in the case of an *a priori* known straight crack [11, 12, 14, 15, 16].

The extended finite element method (XFEM), proposed in [17] and [18] as a technique to allow arbitrary crack propagation without the need of remeshing, has successfully been applied in the framework of fluid-driven fracture propagation in 2D benchmarks either in combination with CZM [19, 20] or with classical mixed-mode propagation criteria based on the stress field at the crack tip [21]. The extremely challenging implementation of XFEM in the case of a pressurized crack propagating in 3D geometries was done in references [22, 23, 24]. XFEM methods have been verified against analytical solutions for plane-strain [19] and penny-shaped [24] impermeable cracks. The main shortcoming of the XFEM approach lies in cases where there is merging or branching of several cracks [25]. In addition, the suitability of this method for large-scale simulations, and therefore 3D scenarios, remains uncertain due to its unproven scalability [26, 1].

Another approach for describing crack propagation along arbitrary crack paths that has recently received significant attention is the phase-field model [27, 28, 29]. Instead of modeling the displacement discontinuity explicitly, phase-field models represent the crack surfaces by a scalar field that is responsible for distinguishing between cracked and uncracked states of the material and whose evolution is obtained by energy-minimization principles. Phase-field models are straightforward to implement and have been widely used to simulate complex fracture geometries, as the description of crack branching and merging is natu-

rally accounted for in the model. In the context of fluid-driven fracture propagation, however, the absence of an explicit description of the displacement jump constitutes a severe limitation, as the crack opening is a fundamental variable in the fluid flow equation that strongly controls the nonlinearity in the hydro-mechanical coupling. In a recent paper it was shown that in the limited case where the fluid pressure field is given, the phase field energy functional can be cleverly formulated to account for the work of the pressurizing fluid without the need to compute the crack opening [30]. However, in realistic scenarios the fluid pressure field is not known and the lubrication equation must be solved, which requires that the crack opening be reconstructed precisely. Several heuristic techniques have been proposed to approximate the displacement jump based on the phase field, see for example [31, 32, 33, 34], although a sound procedure to do so has not been developed yet [1]. Recent attempts combine the benefit of the smeared phase field formulation with a sharp description of the crack [35], but this approach has not been applied to fluid-filled fracture yet.

In this paper we introduce a computational framework that addresses some of the most important challenges in the modeling of fluid-driven fracture propagation: the emergence of arbitrary crack geometries, including crack branching, coalescence, and interaction with pre-existing cracks, and the requirement of massive parallel scalability owing to the inherently three-dimensional nature of the problem in practical applications. Some of the existing limitations and remaining challenges were also identified in [1]. We follow a fully-coupled formulation of the mathematical model and a numerical discretization similar to [12], which employed a combination of finite elements (2D for the solid, 1D for the fluid) and a cohesive zone model to describe crack propagation. The approach was proven very promising as it was verified against the analytical solutions available in several regimes. However, the computational framework assumed a predefined straight crack in 2D propagating under plane-strain conditions. Here we propose a number of modifications to that approach, allowing for unspecified fracture path and enabling high resolution simulations in 3D. To this end, we adopt the Discontinuous Galerkin / Cohesive Zone Model (DG/CZM)

framework originally proposed in [26, 36] for the massively parallel simulation of dynamic fracture and fragmentation of brittle solids. In that approach, the flux and stabilization terms arising at interelement boundaries from the DG formulation prior to fracture are enforced via interface elements. Upon the onset of fracture, the Traction-Separation Law (TSL) governing the fracture process becomes operative without the need to insert a new cohesive element. A key feature of the method is that it avoids the need to propagate topological changes in the mesh as cracks and fragments develop, which enables the indistinctive treatment of crack propagation across processor boundaries and, thus, the scalability of the method to thousands of processors and billion degrees of freedom in explicit dynamics calculations [26]. For the discretization of the lubrication equation we adopt, as in [12], a standard continuous Galerkin finite element formulation whose support is the solid interface elements that have experienced complete failure.

The application of the DG/CZM approach to fluid-driven fracture propagation has recently gained some traction in the community [37, 38]. In those contributions the authors tackle the dynamic problem with either explicit [37] or implicit [38] time integration and a weak coupling of the elasticity and fluid flow equation. Both approaches introduce severe restrictions on the stable time step and, therefore, impose limitations on the accessible time scales, which are in practical terms reduced to subseconds. Although such limitations can sometimes be mitigated by the use of different techniques, including dynamic relaxation, mass scaling, or introduction of artificial numerical dissipation, such type of approach is most useful in specific applications that require the description of the stress waves emanating from the crack tips as they propagate, for example in micro seismic analysis. In the case of field operations of hydraulic fracturing, whose time scales are in the order of minutes or hours and where one is not interested in dynamic effects as the process is inherently quasi-static (fracture growth is stable because it is volume controlled [1]), a quasi-static simulation method is desirable if not mandatory. The main focus of this paper is to enable robust quasi-static simulations of fluid-driven fracture propagation.

The system of strongly nonlinearly coupled equations resulting from the discretization is assembled and solved in parallel with a robust fully-coupled iterative algorithm. A fully-coupled treatment of the coupled system is paramount in the solution of the quasi-static problem. It properly exposes the strong nonlinearity of the coupled system owing to the cubic dependence of the conductivity in the flow equations. It also clearly exposes the parabolic character of the system, thus allowing for natural inflow boundary conditions in a mathematically and numerically-sound manner. Previous approaches based on staggered iteration between the fluid and solid problems [11, 19, 39, 38] are mired with numerical problems whose root is the inconsistent linearization of the coupled nonlinear problem into two weakly-coupled linear ones, and the artificial ellipticity inherited in this case by the fluid problem, which forces the need for an also-artificial essential boundary condition on the pressure. It bears emphasis that all these issues disappear in the fully-coupled treatment of the coupled quasi-static system, as the problem retains its parabolic nature and the system only requires a single boundary condition which can be indistinctively of a Dirichlet or Neumann nature. We will further show via numerical examples that the staggered approach fails even in the case of applied pressure near the crack tip, due to the incorrect numerical treatment of the strong nonlinear dependence of the inflow boundary condition on the crack opening at the mouth.

We conduct a series of numerical tests to verify the computational framework against known analytical solutions for plane-strain and axisymmetric cracks in both the viscosity and toughness dominated regimes. An important finding is that the proposed method results in fluid pressure distributions that are in excellent agreement with the theoretical predictions, even in the case of a *zig-zag* fracture path. This settles a concern that has been recently raised [1]. We also use the case of the interaction of a propagating fluid-driven crack with a pre-existing dry crack as a benchmark to demonstrate that the proposed computational framework is able to describe fracture branching and merging robustly. We finally demonstrate the parallel scalability of the framework up to 30 million degrees of freedom on a 700 processors distributed memory machine.

The present work is structured as follows. In Section 2 we formulate the model with the relevant governing equations. In Section 3 we present the discretizations of the solid and the fluid, with particular focus on the hybrid formulation of the solid (DG/CZM) and fluid (conventional continuous finite elements) and on the fully-coupled iterative algorithm to solve the resulting nonlinear coupled discrete system. In Section 4 we verify the framework against available analytic solutions and we present results demonstrating its robustness and parallel scalability. Conclusions are drawn in Section 5.

2. Governing equations

For completeness, we review the governing equations that describe the hydro-mechanical coupling of a fractured solid when a pressurized fluid is allowed to flow within the crack walls, see also [12]. We consider an impermeable brittle elastic medium and assume a fluid is injected in the solid cracks at a constant rate. The stress field in the solid and the fluid flow are tightly coupled in the following way: the fluid applies a pressure on the crack walls of the solid, whereas the crack geometry (opening and length) constitutes the fluid domain and therefore affects the fluid flow. The description of this two-way coupling requires the formulation of the governing equations for the elastic deformation of the solid material, the laminar flow of the fluid in the cracks, and the propagation of cracks resulting from the stress field in the solid.

We denote with $\Omega \subset \mathbb{R}^d, d = 2, 3$ the solid domain and with $\Gamma^+, \Gamma^- \subset \partial\Omega$ the crack lips, as in Figure 1. As the fluid exerts a pressure p on the crack lips, the following equations state the equilibrium of the solid:

$$\left\{ \begin{array}{ll} -\nabla \cdot \boldsymbol{\sigma} = \mathbf{0} & \text{in } \Omega \\ \boldsymbol{\sigma} \mathbf{n} = -p \mathbf{n} & \text{on } \Gamma^+ \cup \Gamma^- \\ \boldsymbol{\sigma} \mathbf{n} = \bar{\mathbf{t}} & \text{on } \partial\Omega_N \\ \mathbf{u} = \bar{\mathbf{u}} & \text{on } \partial\Omega_D \end{array} \right., \quad (1)$$

where $\boldsymbol{\sigma}$ is the Cauchy stress tensor and \mathbf{u} the displacement field of the solid. In

(1), $\partial\Omega_N$ and $\partial\Omega_D$ denote a partition of $\partial\Omega \setminus (\Gamma^+ \cup \Gamma^-)$, where far field traction $\bar{\mathbf{t}}$ and imposed displacement $\bar{\mathbf{u}}$ are prescribed, respectively.

Small deformations and linear elasticity are commonly employed to model the behavior of the solid prior to fracture. More precisely, the stress field $\boldsymbol{\sigma}$ is related to the deformation by $\boldsymbol{\sigma} = \mathcal{C}\boldsymbol{\varepsilon}(\mathbf{u})$, where \mathcal{C} is the fourth order elasticity tensor and $\boldsymbol{\varepsilon}(\mathbf{u}) = \frac{1}{2}(\nabla\mathbf{u} + \nabla\mathbf{u}^T)$ is the infinitesimal strain.

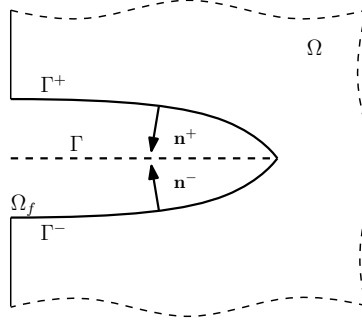


Figure 1: *Sketch of the crack geometry in 2D. The crack lips are Γ^+ and Γ^- and the medium line of the crack Γ .*

The fluid domain $\Omega_f \subset \mathbb{R}^d$, is delimited by Γ^+ and Γ^- as shown in Figure 1. The assumptions of laminar flow and small crack openings w relative to the crack length ℓ justify the use of Reynolds lubrication theory to model the fluid flow. For the purpose of this paper, we do not account for fluid leaving the crack and flowing into the surrounding medium and assume the fractured solid to be impermeable. The model can be extended to account for fluid leak-off adding a time dependent sink term given by Carter's equation [40] as in [12] or employing a generalization of the lubrication equation that explicitly models fluid mass exchange between the crack and the surrounding medium [41]. The governing equations for the fluid flow read:

$$\begin{cases} -\nabla_\Gamma \cdot \left(\frac{w^3}{12\mu} \nabla_\Gamma p \right) = -\frac{\partial w}{\partial t} & \text{in } \Gamma \\ \frac{w^3}{12\mu} \nabla_\Gamma p \cdot \mathbf{n} = Q_0 & \text{on } \partial\Gamma_{in} \end{cases}, \quad (2)$$

where $\Gamma \subset \mathbb{R}^{d-1}$ is the medium crack surface identifying the fluid manifold, w

denotes the opening of the crack, and ∇_Γ the tangential gradient operator on Γ . In (2), $\partial\Gamma_{in} \subset \mathbb{R}^{d-2}$, is the inflow part of the boundary of Γ where fluid is injected at a constant volumetric rate Q_0 , and μ denotes the fluid dynamic viscosity.

The coupling of the fluid flow and the elastic deformations of the surrounding medium are manifested in the mechanical equilibrium requirement at the fluid-solid interface, Equation (1), and in the continuity requirement that the crack opening be equal to the normal component of the displacement jump:

$$w = \llbracket \mathbf{u} \rrbracket \cdot \mathbf{n}_\Gamma, \quad (3)$$

being $\llbracket \bullet \rrbracket$ the jump operator $\llbracket \bullet \rrbracket := \bullet^+ - \bullet^-$ and $\mathbf{n}_\Gamma = \mathbf{n}^- \simeq -\mathbf{n}^+$ the normal to Γ . While in Equation (1) the coupling with the fluid flow appears only in the boundary conditions, the coupling of Equation (2) with the solid mechanics is three-fold: 1) through the (cubic) dependence of the conductivity coefficient in the lubrication equation on the opening; 2) through the modification of the fluid domain Γ as the crack propagates; 3) through the contribution of the local time rate of change of the opening as a sink term in the lubrication equation.

Note that no boundary condition is prescribed at the crack tip, as Equation (2) becomes degenerate for $w = 0$ and the natural boundary condition $w^3 \nabla_\Gamma p \cdot \mathbf{n} = 0$ is identically satisfied [10]. The absence of Dirichlet boundary conditions has raised doubts about the well posedness of the boundary value problem (2) [11, 19, 39]. However, the issue of the nonuniqueness of pressure fields satisfying Equation (2), which results from the formulation of an elliptic boundary value problem without essential boundary conditions, disappears when this equation is fully coupled with the solid mechanics through (1) and (3), that is when the parabolic character of the equation is exposed.

As more and more fluid is injected in the cracks, the fluid pressure increases. A higher fluid pressure in the neighborhood of the crack tip leads to a higher opening stress, which may lead to crack propagation. We assume that the fluid pressure is at all times balanced by the stress field in the solid, so that the resulting crack propagation is quasi-static. As in [12], we employ a Cohesive

Zone Model (CZM), originally proposed in [42] and [43], to describe the quasi-static fracture propagation. We employ a linear traction separation law (TSL) [44] to relate the normal traction \mathbf{t} to the crack opening w as follows:

$$\mathbf{t}(w) = \sigma_c \left(1 - \frac{w}{\delta_c}\right) \mathbf{n}_\Gamma, \quad (4)$$

where δ_c is the length of the cohesive zone and σ_c is the critical stress for which the TSL is activated. Note that with this choice the fracture energy G_c is given by

$$G_c = \frac{1}{2} \sigma_c \delta_c.$$

3. Computational framework

The numerical formulation for the coupled problem (1)-(2)-(4) consists of several ingredients and includes the spatial discretization of the solid mechanics and of the fluid flow. The main characteristic of the solid spatial discretization is that we generalize the DG/CZM framework proposed in [26, 36] for the dynamic propagation of dry cracks to the case of quasi-static propagation of fluid-filled cracks. The DG/CZM method is based on the combination of a discontinuous Galerkin formulation of the continuum problem and a cohesive zone model of fracture. In this framework, the flux and stabilization terms arising from the DG formulation at interelement boundaries are enforced via interface elements, much like in the conventional intrinsic cohesive element approach, albeit in a way that guarantees consistency and stability prior to fracture. Upon the onset of fracture, the TSL governing the fracture process becomes operative without the need to insert a new cohesive element. The main appeal of this approach lies in the consistent weak enforcement of traction continuity at interelement boundaries prior to fracture and the ease of introduction of the cohesive model as fracture occurs, which allows to model fracture propagation on arbitrary meshes.

To describe the fluid flow into the newly created channels as the cracks propagate and expand we adopt a continuous Galerkin finite element discretization

whose support is the set of (d-1)-dimensional interface elements. Figure 2 shows a schematic of the domain: the DG discretization of the bulk material in blue, and all the channels in which the fluid could potentially flow as cracks propagate in the red wireframe.

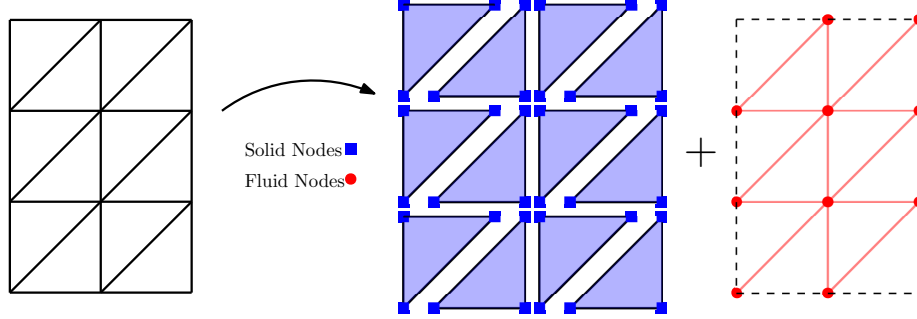


Figure 2: The solid is described on bulk elements and the fluid on the wireframe of the solid discretization. While the bulk finite elements are discontinuous, the interface finite elements are continuous.

We introduce a partition $\{\Omega_h^e\}_{e=1,\dots,N_e}$ of the reference computational domain Ω_h , and we denote with $\partial_I \Omega_h := \cup_{e=1}^{N_e} \partial \Omega_h^e \setminus \partial \Omega_h$ the internal boundary induced by the partition. We denote by $\{\partial \Omega_h^i\}_{i=1,\dots,N_i} \subset \partial_I \Omega_h$, the set of elements belonging to the interelement boundary of the partition $\{\Omega_h^e\}$. The semi-discrete displacement and pressure fields are approximated as $\mathbf{u}_h = \sum_{j=1}^{N_u} u_j \boldsymbol{\varphi}_j$ and $p_h = \sum_{j=1}^{N_p} p_j \eta_j$, respectively, where $\{\boldsymbol{\varphi}_i\}_{i=1,\dots,N_u}$ and $\{\eta_i\}_{i=1,\dots,N_p}$ are bases of \mathcal{U}_h and \mathcal{P}_h , the conventional interpolation spaces of discontinuous Galerkin and continuous Galerkin finite elements, respectively:

$$\begin{aligned} \mathcal{U}_h &= \left\{ \mathbf{v}_h \in \mathbf{L}^2(\Omega_h) : \quad \mathbf{v}_h|_{\Omega_h^e} \in \mathbf{P}^k(\Omega_h^e) \quad \forall e = 1, \dots, N_e \right\}, \\ \mathcal{P}_h &= \left\{ q_h \in C^0(\partial_I \Omega_h) : \quad q_h|_{\partial \Omega_h^i} \in \mathbf{P}^k(\partial \Omega_h^i) \quad \forall i = 1, \dots, N_i \right\}. \end{aligned}$$

We also introduce, for the sake of notation, the discrete crack opening $w_h := \llbracket \mathbf{u}_h \rrbracket \cdot \mathbf{n}_\Gamma$ on $\partial_I \Omega_h$. The discrete formulation of (1)-(4) is obtained testing

equations (1) and (2) against \mathbf{v}_h and q_h , respectively, resulting in:

$$\begin{aligned}
& \sum_e \int_{\Omega_h^e} \mathcal{C} \boldsymbol{\varepsilon}(\mathbf{u}_h) : \boldsymbol{\varepsilon}(\mathbf{v}_h) \, dV \\
& + \int_{\partial_I \Omega_h} (1 - \alpha_h) \left(\{ \mathcal{C} \boldsymbol{\varepsilon}(\mathbf{u}_h) \} \llbracket \mathbf{v}_h \rrbracket \cdot \mathbf{n}_\Gamma + \frac{b}{h} \llbracket \mathbf{v}_h \rrbracket \otimes \mathbf{n}_\Gamma : \mathcal{C} : \llbracket \mathbf{u}_h \rrbracket \otimes \mathbf{n}_\Gamma \right) \, dS \\
& + \int_{\partial_I \Omega_h} (\alpha_h \mathbf{t}(w_h) - \beta_h p_h \mathbf{n}_\Gamma) \cdot \llbracket \mathbf{v}_h \rrbracket \, dS + \\
& = \sum_e \int_{\partial \Omega_h^e \cap \partial \Omega_N} \bar{\mathbf{t}} \cdot \mathbf{v}_h \, dS \quad \forall \mathbf{v}_h \in \mathcal{U}_h,
\end{aligned} \tag{5}$$

$$\int_{\partial_I \Omega_h} \beta_h \left(\frac{w_h^3}{12\mu} \nabla_\Gamma p_h \cdot \nabla_\Gamma q_h + \frac{\partial w_h}{\partial t} q_h \right) \, dS = \int_{\partial \Gamma_{in}} Q_0 q_h \, dL \quad \forall q_h \in \mathcal{P}_h, \tag{6}$$

where $\{\bullet\} := \frac{1}{2}(\bullet^+ + \bullet^-)$ denotes the average operator. In Equation (5), the first term represents the usual contribution of the bulk stresses to the virtual work. The second line of Equation (5) consists of the various internal boundary terms resulting from the DG discretization, including the consistency and the stabilization terms [45, 46]: the first term ensures the consistency of the numerical scheme and comes as a boundary contribution from the integration by parts on each element Ω_h^e , whereas the second terms weakly enforces displacement continuity at element interfaces with a stabilization parameter b relative to the mesh size h . As in [26], the factor α_h is added to control the activation of the TSL: $\alpha_h = 0$ before the onset of fracture and $\alpha_h = 1$ after the stress reaches the prescribed critical value σ_c . The third line of Equation (5) is therefore active after the onset of fracture and accounts for the virtual work of the cohesive tractions as well as the natural boundary condition applied by the fluid. Similarly to α_h , β_h is a binary field that allows to activate the fluid domain when actual flow conditions are achieved, *e.g.* outside the fluid-lag region behind the crack tip. This allows to incorporate different models of fluid-lag, as described below. Finally, the last line of Equation (5) accounts for the natural boundary condition in the remote boundary.

It bears emphasis that, regardless of the occurrence of fracture propagation,

the hydro-mechanical coupling of equations (5) and (6) is extremely stiff due to the nonlinear dependence of the lubrication conductivity on the crack opening displacement. In order to minimize the issues of numerical robustness we adopt a fully-coupled solution strategy. We propose an iterative algorithm to advance the coupled problem (5)-(6) in time. We employ a first order discretization of the time derivative in Equation (6), where the displacement and pressure fields are treated implicitly. More precisely, we discretize $\frac{\partial w_h}{\partial t}$ at time t^{n+1} as:

$$\left. \frac{\partial w_h}{\partial t} \right|_{t^{n+1}} \approx \frac{w_h^{n+1} - w_h^n}{\Delta t},$$

where Δt is the time step for the integration. The resulting fully-discrete system reads:

$$\begin{aligned} & \sum_e \int_{\Omega_h^e} \mathcal{C} \varepsilon(\mathbf{u}_h^{n+1}) : \varepsilon(\mathbf{v}_h) \, dV + \int_{\partial_I \Omega_h} (\alpha_h^{n+1} \mathbf{t}(w_h^{n+1}) - \beta_h^n p_h^{n+1} \mathbf{n}_\Gamma) \cdot \llbracket \mathbf{v}_h \rrbracket \, dS \\ & + \int_{\partial_I \Omega_h} (1 - \alpha_h^{n+1}) \left(\left\{ \mathcal{C} \varepsilon(\mathbf{u}_h^{n+1}) \right\} \llbracket \mathbf{v}_h \rrbracket \cdot \mathbf{n}_\Gamma + \frac{b}{h} \llbracket \mathbf{v}_h \rrbracket \otimes \mathbf{n}_\Gamma : \mathcal{C} : \llbracket \mathbf{u}_h^{n+1} \rrbracket \otimes \mathbf{n}_\Gamma \right) \, dS \\ & = \sum_e \int_{\partial \Omega_h^e \cap \partial \Omega_N} \bar{\mathbf{t}} \cdot \mathbf{v}_h \, dS \quad \forall \mathbf{v}_h \in \mathcal{U}_h, \end{aligned} \tag{7}$$

$$\begin{aligned} & \int_{\partial_I \Omega_h} \beta_h^n \left(\frac{(w_h^{n+1})^3}{12\mu} \nabla_\gamma p_h^{n+1} \cdot \nabla_\gamma q_h + \frac{w_h^{n+1}}{\Delta t} q_h \right) \, dS \\ & = \int_{\partial \Gamma_{in}} Q_0 q_h \, dL + \int_{\partial_I \Omega_h} \beta_h^n \frac{w_h^n}{\Delta t} q_h \, dS \quad \forall q_h \in \mathcal{P}_h, \end{aligned} \tag{8}$$

where \mathbf{u}_h^{n+1} , p_h^{n+1} are the unknown displacement and pressure at time t^{n+1} and w_h^n is the opening at time t^n .

System (7)-(8) constitutes a fully-coupled nonlinear algebraic system in the nodal unknowns $\mathbf{U} = \{u_i\}_{i=1}^{N_u}$ and $\mathbf{P} = \{p_i\}_{i=1}^{N_p}$, whose solution propagates their known values at time t^n to time t^{n+1} . A straightforward linearization of (7)-(8) yields a linear system of equations of the form:

$$\begin{bmatrix} A & B \\ C & D \end{bmatrix} \begin{bmatrix} \mathbf{U} \\ \mathbf{P} \end{bmatrix} = \begin{bmatrix} \mathbf{E} \\ \mathbf{F} \end{bmatrix}. \tag{9}$$

To solve the nonlinear problem we adopt a Newton-Raphson scheme in which the linear system (9) is solved to advance from the nonlinear iteration k to $k+1$ until convergence, starting from initial guesses $w_0^{n+1} = w^n$ and $p_0^{n+1} = p^n$. Convergence is evaluated in the Euclidean norm of the relative increments of both unknown nodal arrays. We find that, even in the presence of the fracture propagation nonlinearity, the Newton-Raphson iterative strategy performed on the fully-coupled system works robustly as long as we do not update β_h until the end of the time step.

We have implemented the proposed computational approach in a framework for large-scale simulations in computational mechanics. Parallel scalability is achieved by partitioning the computational domain among the participating processors using the ParMETIS library [47]. Each processor is then responsible for storing and maintaining the solution information for its portion of the mesh and for assembling its portion of the linear system (9) resulting from the discretization. The efficient and robust solution of the linearized system in each nonlinear iteration was explored using a variety of parallel iterative solvers with preconditioners based on domain decomposition, using the PETSc library [48]. We found that a parallel preconditioned iterative solver based on domain decomposition combined with a direct solver within each subdomain provides excellent robustness and parallel scalability, as we show in Section 4.

Remark 1. *It is well-known that a lag region exists between the fluid front and the crack front, where the fluid pressure is equal to the vapor pressure p_v for an impermeable crack, or to the pore pressure for a crack in a porous medium [1]. It is possible to compute the lag size either analytically in the simple case of a straight crack, or to embed the computation of the lag in the computational approach, as in [49, 39]. The factors controlling the size of the fluid lag are now well-understood: it has been shown that the lag size vanishes exponentially with the increase of nondimensional toughness [50], and decreases for increasing confining stresses [51]. Furthermore, it has been recently shown that under prevailing conditions in field operations of hydraulic fracture the fluid lag is small*

and fully embedded in the fracture cohesive zone [52]. For this reason, in this paper we limit our attention to the case in which the fluid lag is negligible and assume that the fluid permeates the cohesive zone, as was done in [11, 19, 38]. More precisely, we activate the fluid domain when a given crack opening threshold δ_f is achieved and choose $\delta_f \ll \delta_c$, being δ_c the critical opening of the cohesive law. Assuming that the fluid and crack fronts coincide however, exposes the degeneracy of the fluid equations at the crack tip, due to the vanishing opening, which results in a nonintegrable fluid pressure singularity. From the numerical standpoint, this results in the ill-conditioning of the jacobians, which we handle by imposing a cut-off to the fluid pressure to the vapor pressure, as was done multiple times in the past [11, 19, 38].

4. Results

In order to assess the numerical properties of the computational framework, we conduct a series of numerical tests.

4.1. Verification of the fully-coupled algorithm

In order to verify the proposed computational approach, we conduct a series of numerical tests that attempt to replicate the analytical solutions available for a wide range of physical regimes for fluid-driven straight cracks. Specifically we consider a straight crack immersed in a solid under plane strain conditions subject to fluid pressure resulting from inflow (Neumann) boundary conditions. This problem was originally formulated in [3, 4] and historically referred to as the *KGD* model. Depending on the relative values of the model parameters, *i.e.* the plane-strain Young's modulus E' , the critical fracture energy release rate G_c , the fluid injection rate Q_0 , and the fluid viscosity μ , two different propagation regimes can emerge for an impermeable crack where analytical solutions have been found [53]. As part of the derivation of the solution of the KGD problem it has been found that two nondimensional parameters dictate the specific solution

regime: the nondimensional toughness \mathcal{K} and the nondimensional viscosity \mathcal{M} :

$$\mathcal{K} = \left(12\mu Q_0 (E')^3\right)^{-\frac{1}{4}} \frac{8}{\sqrt{2\pi}} K_{IC},$$

and

$$\mathcal{M} = 12\mu Q_0 (E')^3 \left(\frac{8}{\sqrt{2\pi}} K_{IC}\right)^{-4},$$

where $K_{IC} = \sqrt{G_c E'}$ is the critical stress intensity factor under plane strain and mode I propagation conditions [54]. Physically \mathcal{K} and \mathcal{M} represent the importance of fracture and viscous flow, respectively, as the main dissipation mechanism. It should be noted that $\mathcal{K} = \mathcal{M}^{-1/4}$, which highlights the fact that these two mechanisms are actually in competition [53].

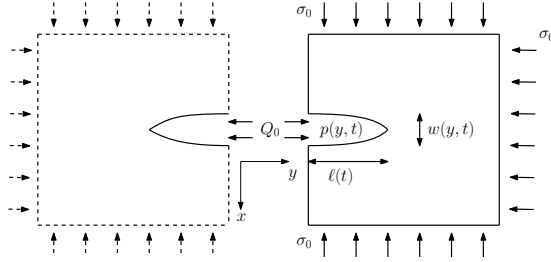


Figure 3: *The plain-strain configuration of the fluid-driven fracture. Exploiting symmetry, we focus on half of the domain.*

In the case that viscous effects dominate (*viscosity-dominated* regime, large \mathcal{M} , low \mathcal{K}) the analytical solution presents a near-tip boundary layer [8]. This is due to incompatibility of the near-tip behavior of the zero-toughness solution with the tip asymptote prescribed by linear elastic fracture mechanics for any small, yet nonzero, toughness. The zero-toughness solution is known to have a weakly singular near-tip asymptote characterized by the 2/3-power dependence of the fracture opening on the distance from the tip, while the pressure field is singular at the tip with a $-1/3$ power. Conversely, when the main dissipation mechanism is fracture propagation (*toughness-dominated* regime, low \mathcal{M} , large \mathcal{K}), the zero-viscosity pressure solution is uniform, whereas a tip-singularity is present in the pressure only in higher order terms [55]. Threshold values delimiting the two regimes have been obtained by Garagash, Detournay *et al.*

with the result that $\mathcal{K} < \mathcal{K}_0 = 0.70$ corresponds to the viscosity-dominated regime [8], and $\mathcal{K} > \mathcal{K}_\infty = 4.13$ corresponds to the toughness-dominated regime [55]. For intermediate values of \mathcal{K} , transition between regimes occurs, although it is important to note that a plane-strain fracture cannot transition from one regime to one another during its time evolution, since \mathcal{K} and \mathcal{M} do not depend on time [53].

	viscosity regime	toughness regime
E	17 GPa	17 GPa
ν	0.2	0.2
μ	0.1 Pa s	10 μ Pa s
Q_0	0.001 $m^2 s^{-1}$	0.001 $m^2 s^{-1}$
G_c	120 Pa m	120 Pa m
\mathcal{K}	0.51	5.1
\mathcal{M}	14	0.0014

Table 1: *The parameters used in the simulations with the corresponding nondimensional toughness \mathcal{K} and viscosity \mathcal{M} . The left-hand set of parameters corresponds to the viscosity-dominated regime, whereas the right-hand set of parameters corresponds to the toughness-dominated regime.*

In order to test the computational framework in both regimes, we select two representative cases corresponding to the parameters shown in Table 1. Once the parameters are chosen, the analytical solutions provide the crack length, pressure distribution, and crack opening distribution as a function of time, respectively $\ell(t), p(y, t), w(y, t)$. We extract the functional forms of these solutions from [8] in the case of the viscosity-dominated regime, and from [55] in the case of the toughness-dominated regime.

As an initial step, we verify that the computed and theoretical pressure and opening distributions are consistent for a crack of given length $\bar{\ell}$ embedded in the computational mesh, by performing the calculations of one time step, which advance the solutions from time t^n to time t^{n+1} . This enables the assessment

of the properties of the solution of the coupled system (7)-(8) in isolation from the crack propagation algorithm, which will be tested in Section 4.2. It bears emphasis that in order to match the analytical solution at time t^{n+1} , Equation (8) requires the analytical opening w^n at time t^n , which is maintained fixed as a source term during the nonlinear iteration process. By contrast, we have freedom in the choice of the initial guesses of the pressure and opening fields p_0^{n+1} and w_0^{n+1} : although they could be adopted from the previous time step (*i.e.* $w_0^{n+1} = w^n$ and $p_0^{n+1} = p^n$), we have found that the convergence is very fast and robust even if the initial guess is very far from the analytic solution. In order to demonstrate robustness, our calculation below starts from uniform distributions $w_0^{n+1} = w^0$ and $p_0^{n+1} = p^0$.

For each regime, we test the algorithm for four initial crack lengths $\bar{\ell} = 5m, 6m, 7m, 8m$. To make sure that the computational domain is large enough to support the infinite hypothesis, we construct the computational domain $[0, 45m] \times [0, 60m]$. We exploit the symmetry of the problem and apply half the injection rate $\frac{Q_0}{2}$. The mesh is refined in the proximity of the crack tip, where the mesh size is $h = 0.1m$, the polynomial order of the finite elements is $p = 2$. We have found the choice of time step $\Delta t = 1s$ for the viscosity-dominated regime and $\Delta t = 0.1s$ for the toughness dominated regime and for the chosen values for the physical parameters the result converge to the analytical solution showing that the right hand side of equation (2) is properly resolved. For simplicity, we adopt $\bar{\mathbf{t}} = \mathbf{0}$ (no far-field stress). Finally, in both regimes, the uniform initial guesses for pressure and opening are $p^0 = 1MPa$ and $w_0 = 2mm$.

Figures 4 and 5 show comparisons of the numerical solutions with the analytical ones in the viscosity and toughness-dominated regimes, respectively. We observe that the numerical solution is in excellent agreement with the analytical predictions. We also observe that as the initial crack increases the assumption of infinite domain is not represented by the computational domain.

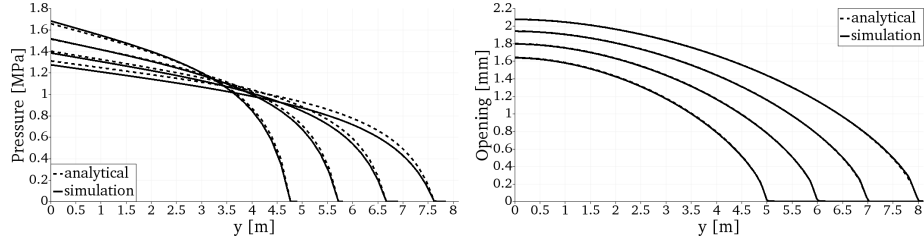


Figure 4: Comparison of the computational predictions against the analytical solutions in the viscosity-dominated regime from [8] for several crack lengths 5m, 6m, 7m, 8m.

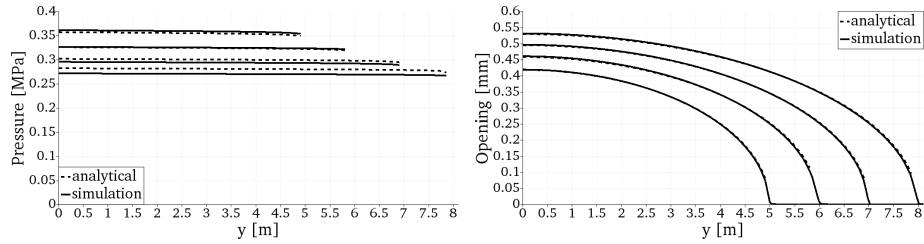


Figure 5: Comparison of the computational predictions against the analytical solutions in the toughness-dominated regime from [55] for several crack lengths 5m, 6m, 7m, 8m.

4.2. Verification of the crack propagation algorithm

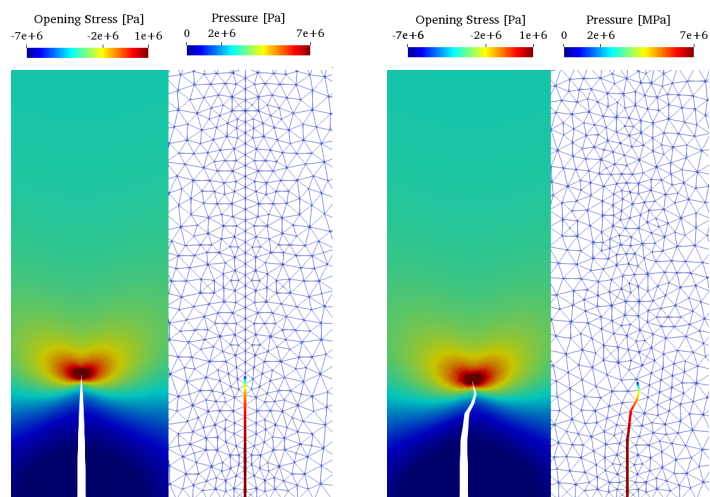
In our next test we evaluate the performance, robustness, and accuracy of the crack propagation algorithm. Describing numerically the nonlinearities coming from the softening response as the crack propagates, on top of the nonlinearity of the fluid-solid coupling, is extremely challenging, especially under quasi-static conditions. In addition, we explore the possible implications of the restrictions in the crack paths imposed by the DG/CZM approach. To be more precise, in the proposed framework cracks are allowed to propagate on the solid element interfaces. Hence, a given mesh provides a finite number of potential crack paths, which may or may not include the exact crack path. The concern about whether a potential *zig-zag* path of the crack can produce a reasonable fluid pressure distribution has been raised in [1]. We therefore consider two different meshes: one mesh contains the straight analytical crack path, the other mesh is unbiased.

We consider the same case in the viscosity-dominated regime from section 4.1, except that in this case we consider a far-field stress of the form $\bar{\mathbf{t}} = -\sigma_0 \mathbf{n}$ to replicate more realistic field conditions with $\sigma_0 = 4.0 \text{ MPa}$. Following [12], we set the fracture stress in Equation (4) to $\sigma_c = 1.0 \text{ MPa}$. The initial crack length is $\bar{\ell} = 0.5 \text{ m}$, which corresponds to $t^0 = 0.4 \text{ s}$. Both computational meshes are uniformly refined along the expected crack path direction, with a characteristic mesh size $h = 0.1 \text{ m}$, and coarsened elsewhere. The polynomial order of the finite elements is $p = 3$.

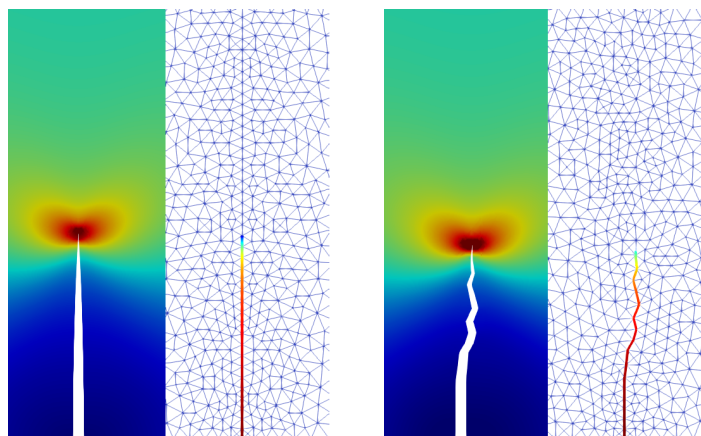
The solution procedure is done according to the nonlinear solution described in Section 3 with a time step $\Delta t = 0.025 \text{ s}$ until the final time of 60 s , that is a final crack length of approximately 15 m . We observed that the Newton-Raphson procedure converges robustly in typically 3 to 5 iterations in time steps where the crack does not propagate, and in 5-10 iterations when the crack propagates.

Figure 7 shows snapshots comparing side by side the results obtained on the two different meshes for selected simulation times in the time range $t \in [1 \text{ s}, 5 \text{ s}]$ in a close-up view of size $1.3 \text{ m} \times 3.5 \text{ m}$ near the injection point. The left figures show contours of the opening stress field. In order to expose the crack path, the deformations are magnified by a factor of 100. The right figures show the wireframe of the fluid domain: the blue segments constitute inactive fluid elements, whereas the colored segments constitute the active fluid domain, where the color represents the fluid pressure. It is interesting to observe that although the crack at this scale does exhibit a *zig-zag* behavior, the macroscopic response qualitatively hardly differs from the straight path, as shown in Figure 8.

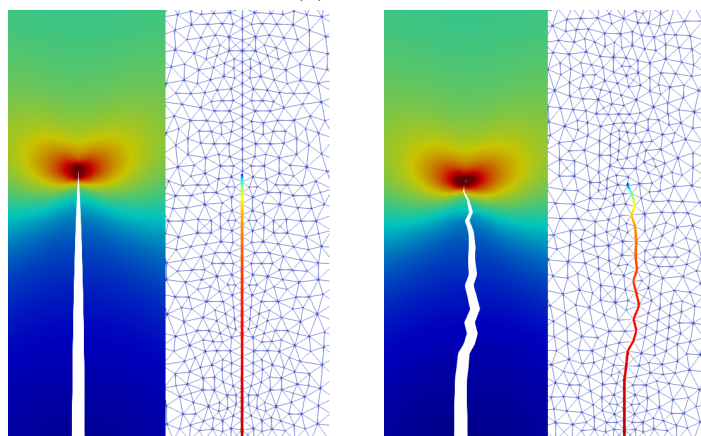
Figure 9 compares the time evolution of the net pressure, $p - \sigma_0$, and opening w at the crack mouth (*i.e.* at the injection point) obtained with the two different meshes with the analytical solution from [8]. In both cases, the results are in good agreement with the analytical solution.



(a) $t = 1.0s$



(b) $t = 2.0s$



(c) $t = 3.0s$

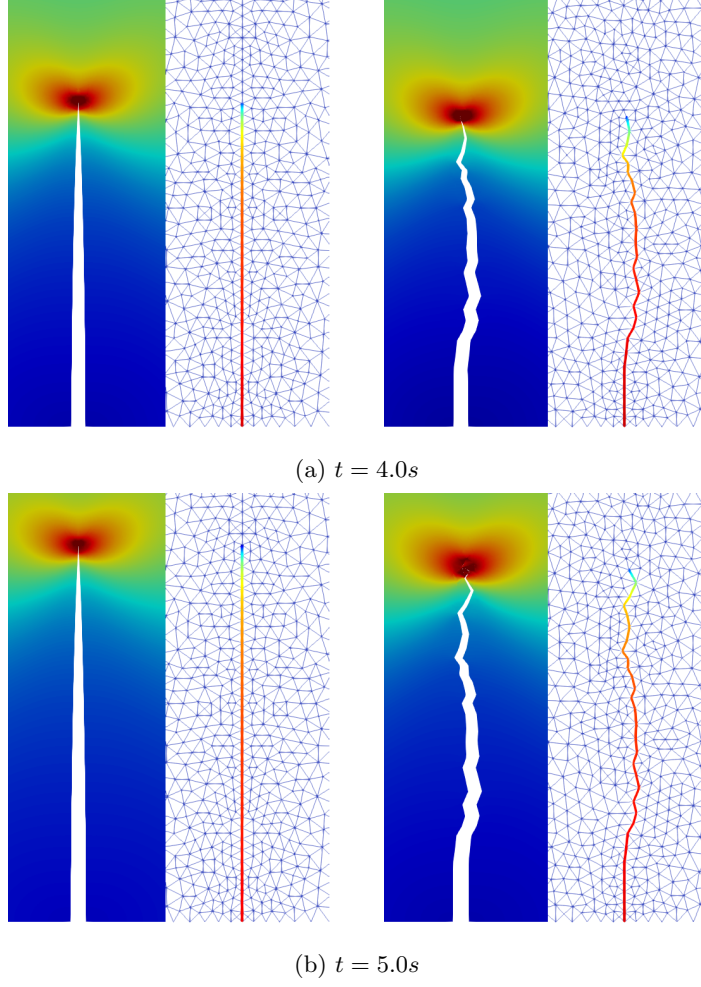


Figure 7: *Simulation results corresponding to the viscosity-dominated regime according to the parameters given in Table 1 obtained with two different meshes. Each row corresponds to a different simulation time and shows snapshots obtained on an arbitrary mesh (left snapshot) and on a biased mesh (right snapshot). In each snapshot, the contour plot on the left shows the opening stress (the solid deformation is magnified by a factor of 100), while the wireframe on the right shows the fluid domain: the blue segments constitute inactive fluid elements, whereas the colored segments constitute the active fluid domain, where the color represents the fluid pressure. Note that, if the straight path is included in the set of potential paths.*

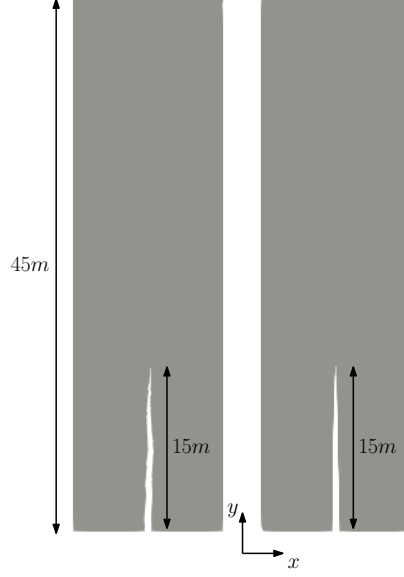


Figure 8: *Qualitative comparison of the macroscopic crack path obtained with the arbitrary mesh (left picture) and on the biased mesh (right picture) at the final time $t = 60$ s (final crack length 15 m). Note that the crack paths obtained on the two meshes are in very good agreement. The crack opening is magnified of a factor of 500.*

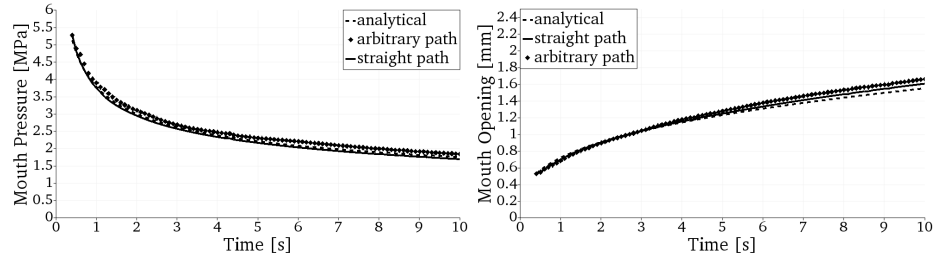


Figure 9: *Time evolution of the mouth net pressure $p - \sigma_0$ (left) and mouth opening (right) obtained from the simulations with both the arbitrary and the biased meshes in comparison with the analytical solution from [8].*

4.3. Fully-coupled vs. staggered hydro-mechanics with applied inflow boundary conditions

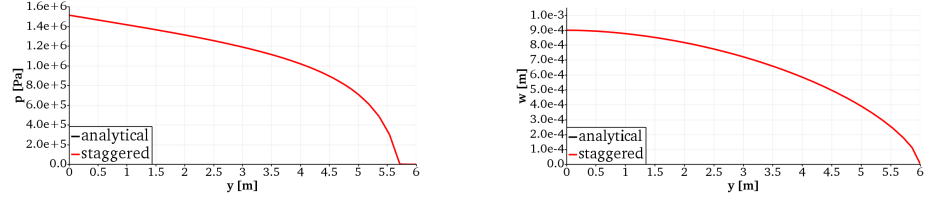
As mentioned in the introduction, the concern about a *staggered* coupling approach has been brought up previously. Here we investigate the limitations of such approach. We revisit the test problem of Section 4.1 and we explore the staggered approach. In this case, Equations (7) and (8) are solved with respect to their primal variable in a sequential iterative manner in which the other unknown required from the equation is taken from the results of the previous iteration: the solid displacements are obtained from Equation (7) using the pressure from the previous iteration; similarly, the pressure is computed from Equation (8) using the crack opening from the previous iteration. Numerically this corresponds to an *ad hoc* linearization of the problem where the linear system (9) above becomes decoupled and of the form $AU = \mathbf{E} - BP, DP = \mathbf{F} - CU$.

It is important to note that under these conditions the discrete system loses its parabolic character. Specifically the decoupled fluid equation becomes elliptic thus requiring a Dirichlet boundary condition, *i.e.* the specification of the pressure at least at one point in the domain. In order to mitigate the problems associated with these deficiencies in the staggered approach, different numerical artifacts have been proposed, including: setting the Dirichlet boundary condition at the mouth of the crack, which is seldom or never representative of hydraulic fracture operations [11], estimating a value for the mouth pressure from the imposed flow [19], applying the fictitious Dirichlet boundary condition near the crack tip using the concept of the fluid lag where the pressure is assumed to be the vapor pressure (in the case of impermeable rock) [39]. In [38], the problem of system ill-posedness is also avoided by enforcing the need to apply Dirichlet boundary conditions at the mouth of the crack.

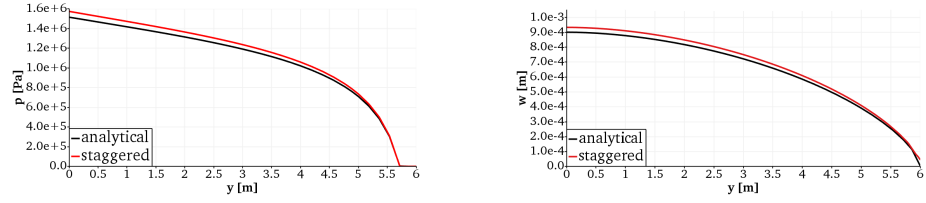
We consider a plane-strain crack as in Section 4.1 with a given initial length $\bar{\ell}$. To be able to impose natural boundary conditions specifying the injection rate at the crack mouth in the fluid boundary value problem resulting from the staggered solver, we need to impose an essential pressure boundary at some

point along the crack. Having at disposal the analytical solution to this problem [8], we choose to impose zero pressure at the point behind the crack tip where the analytical pressure solution is zero, as the problem degeneracy forbids to impose the pressure at the crack tip. Similarly to what we did in Section 4.1, we simulate one time step, advancing from the solution at time t^n to the solution at time t^{n+1} . We initialize the staggered solvers using as old opening w^n the analytical opening field at time t^n . The guesses for opening and pressure, w_0^{n+1} and p_0^{n+1} , can be freely chosen, depending on how far from the analytical solution we want to initialize the two iterative procedures.

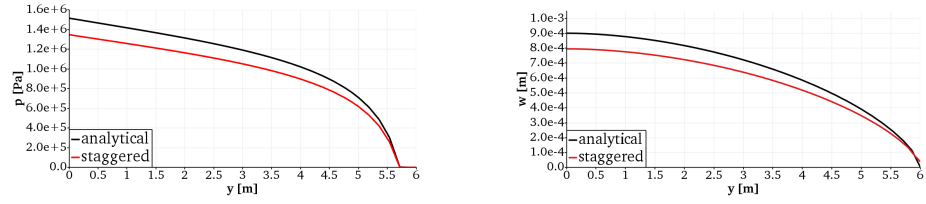
Figures 10 and 11 show the results obtained during the nonlinear iterations with the two solvers, staggered and fully-coupled, starting from an initial crack length $\bar{\ell} = 6m$ and with the set of parameters in Table 1 corresponding to the viscosity-dominated regime. Figure 10 shows that the staggered approach does not converge for inflow boundary conditions, not even using the analytical solutions as initial guesses. This instability can be explained by the activation of vicious-circle mechanism for which a higher pressure obtained from the lubrication equation will result in a higher mouth opening in the elasticity equation that will make the pressure drastically drop at the following fluid iteration. In turn, a lower pressure obtained in the lubrication will result in a lower mouth opening in the elasticity equation that will make the pressure drastically increase at the following fluid iteration. This mechanism disappears in the fully-coupled approach, which computes the opening and pressure at once and with the proper tangents. This is confirmed by our numerical experimentation, which shows robust convergence even starting from initial guesses that are far from the analytical solution, see Figure 11.



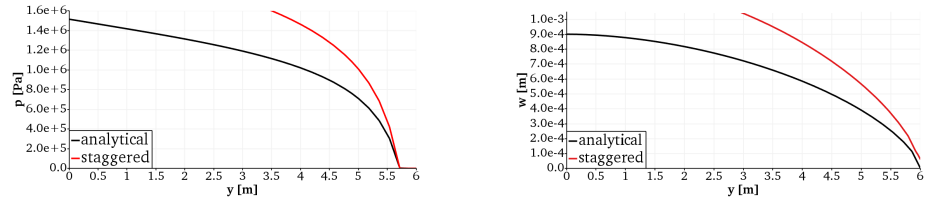
(a) *Initial guess*



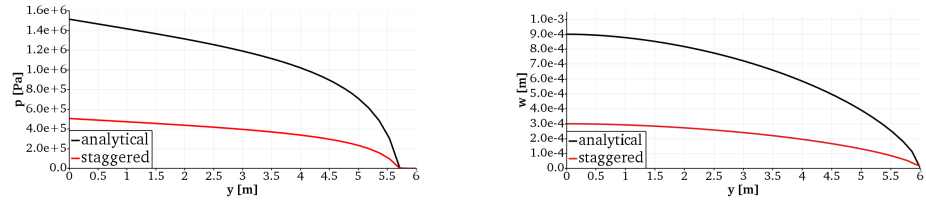
(b) *Iteration 1*



(c) *Iteration 2*

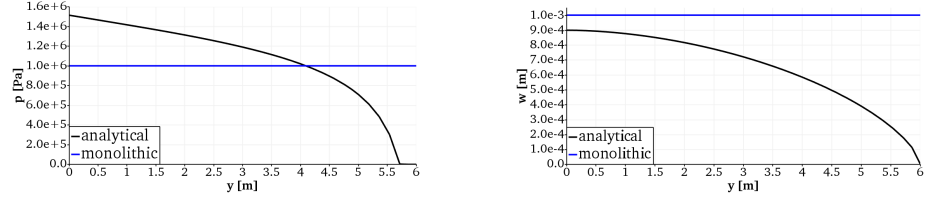


(d) *Iteration 3*

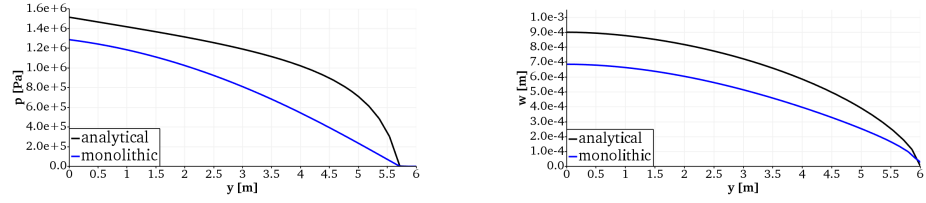


(e) *Iteration 4*

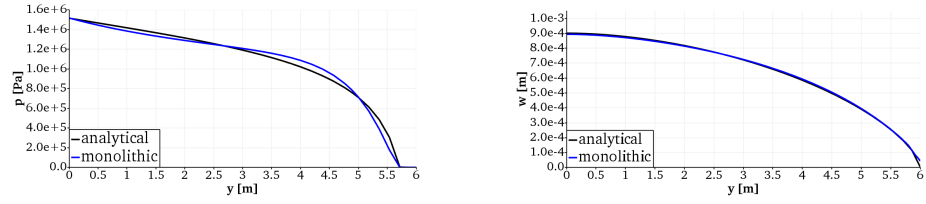
Figure 10: Snapshots of the pressure (left) and crack opening (right) distributions during the staggered nonlinear iteration procedure. The staggered solver diverges even when the initial guess corresponds to the analytical solution.



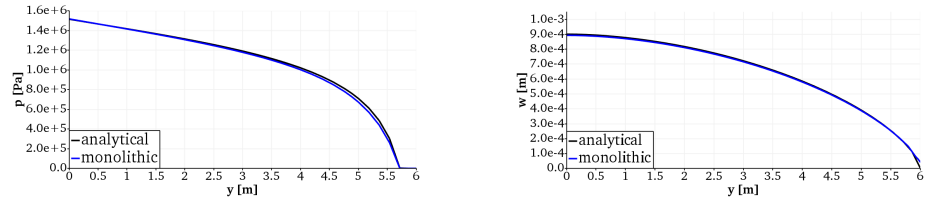
(a) *Initial guess*



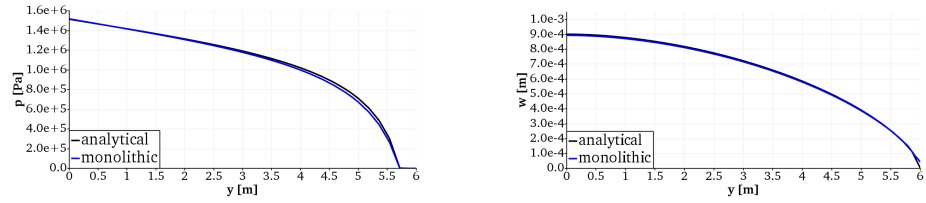
(b) *Iteration 1*



(c) *Iteration 2*



(d) *Iteration 3*



(e) *Iteration 4*

Figure 11: Snapshots of the pressure (left) and crack opening (right) distributions during the fully-coupled nonlinear iteration procedure. The fully-coupled solver converges robustly with respect to the initial guess.

4.4. Verification of the fully-coupled algorithm for a penny-shaped crack in the viscosity dominated regime

In order to exercise the proposed computational framework under three dimensional conditions, we conduct a simulation of a fluid-filled penny-shaped crack in the viscosity dominated regime and compare against the analytical solutions in [56].

For the radial crack geometry, the nondimensional toughness \mathcal{K} and viscosity \mathcal{M} are expressed as:

$$\mathcal{K} = \left(\frac{t^2}{(12\mu)^5 Q_0^3 E'^{13}} \right)^{1/18} \frac{8}{\sqrt{2\pi}} K_{IC},$$

and

$$\mathcal{M} = 12\mu \left(\frac{Q_0^3 E'^{13}}{t^2} \right)^{1/5} \left(\frac{8}{\sqrt{2\pi}} K_{IC} \right)^{-18/5},$$

see [56]. Note that, similarly to the plane-strain crack geometry, \mathcal{K} and \mathcal{M} represent the importance of fracture and viscous flow as the main dissipation mechanism, the competition of these mechanisms being highlighted from the fact that $\mathcal{M} = \mathcal{K}^{-18/5}$. Furthermore, analogously to the case of a plane-strain crack, analytical solutions based on the assumption that the fluid front coincides with the crack tip result in a pressure singularity at the tip. The zero-toughness solution is known to have a weakly singular near-tip fracture opening with a 2/3-power dependence on the distance from the tip, while the pressure field is still singular at the tip with the $-1/3$ -power dependence. In addition to the $-1/3$ -power tip singularity, the pressure field also presents a logarithmic singularity at the injection point [56]. Threshold values delimiting the two regimes have been obtained with the result that $\mathcal{K} < \mathcal{K}_0 = 0.37$ corresponds to the viscosity-dominated regime [55], and $\mathcal{K} > \mathcal{K}_\infty = 3.5$ corresponds to the toughness-dominated regime [56]. However, differently than in the case of a plane-strain crack, for a radial crack \mathcal{K} and \mathcal{M} depend on time, suggesting that transition between regimes may happen during fracture propagation, albeit typically very slowly [56].

We provide verification of the proposed computational framework in the viscosity-dominated regime, see parameters in Table 2, for an axisymmetric

E	17 GPa
ν	0.2
μ	0.15 Pa s
Q_0	0.03 m ³ s ⁻¹
G_c	100 Pa m
\mathcal{K}	0.35
\mathcal{M}	42.4

Table 2: *The parameters used in the simulations with the corresponding nondimensional toughness \mathcal{K} and viscosity \mathcal{M} . Note that \mathcal{K} and \mathcal{M} are time-dependent, hence depend on the crack radius \bar{R} . The values of \mathcal{K} and \mathcal{M} reported in the Table correspond to \bar{R} , that is for a time $t = t^0 = 17.6s$ (see analytic solution in [56]). This set of parameters corresponds to the viscosity-dominated regime.*

crack. Once the parameters are chosen, the analytical solutions provide the crack radius, pressure distribution, and crack opening distribution as a function of time, respectively $R(t), p(r, t), w(r, t)$. We extract the functional forms of these solutions from [56] in the case of the viscosity-dominated regime. Similarly to the analysis done in Section 4.1, we verify that the computed and theoretical pressure and opening distributions are consistent for a crack of given radius \bar{R} embedded in the computational mesh by performing the calculations of one time step, which advance the solutions from time t^n to time t^{n+1} . We choose the initial guesses of the pressure and opening fields p_0^{n+1} and w_0^{n+1} adopting the analytical solution from the previous time step (*i.e.* $w_0^{n+1} = w^n$ and $p_0^{n+1} = p^n$).

In our calculations, we utilize the computational domain $[0, 50m] \times [0, 50m] \times [0, 50m]$. We exploit the symmetry of the problem, being careful to only apply the injection rate $\frac{Q_0}{4}$. The radial fracture lies on the plane $z = 0$ and has an initial radius $\bar{R} = 10m$. The injection point is located at the origin. Consistently with the choice of initial radius, the initial time of the simulation is $t = t^0 = 17.6s$, as prescribed from the analytical solution [56]. Notice that, with the set of parameters summarized in Table 2, the viscosity-dominated regime corresponds to earlier times than 26.8s, whereas the toughness-dominated regime

corresponds to larger times than $16Gs$. This is consistent with the observation in [56] that the toughness-dominated regime is relevant only in exceptional circumstances. The mesh is refined in the proximity of the crack tip, where the mesh size is $h = 0.2m$, the polynomial order of the finite elements is $p = 2$, and the time step is $\Delta t = 1s$.

In Figure 12 we show a section of the fluid domain immersed in the 3D solid domain. Contours of the fluid pressure and the opening stress show the balance between the two at the crack lips, as prescribed by mechanical equilibrium. Figure 13 shows that the opening and the pressure fields are in excellent agreement with the analytical solution from [56].

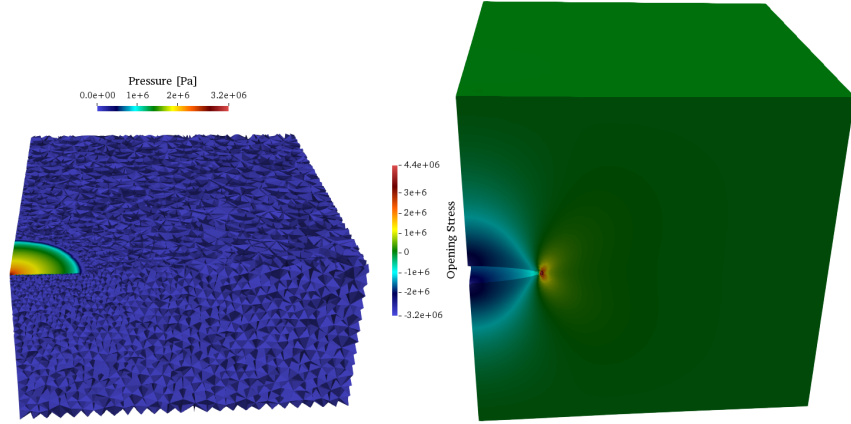


Figure 12: *A slice of the fluid domain (on the left) and the solid domain (on the right) for a penny-shaped crack in 3D with contours of the fluid pressure field and the opening stress, respectively. The fluid equations are solved on the wireframe of the solid mesh.*

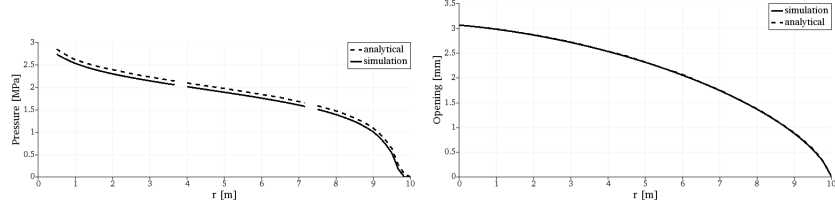


Figure 13: Verification of the computational predictions of the fluid pressure field (left plot) and crack opening field (right plot) for a penny-shaped radial crack (analytical solution from [56]).

4.5. Interaction with a pre-existing crack

The problem of interaction of fluid-driven cracks with pre-existing *natural* cracks is of significant interest in oil field operations. Key questions about this interaction of cracks include whether the natural crack is filled by the injected fluid and therefore activated, or if it is simply crossed by the propagating crack. Several factors contribute to the problem evolution, including the angle of interaction, the *in situ* stress, the injection rate and the viscosity of the fracturing fluid [57].

In this paper we use the problem of interaction of a fluid-driven crack with a natural crack to illustrate the capability of the proposed computational approach to effectively describe branching and merging. We select a case in which a pressurized crack propagates in a domain with a pre-existing dry crack, as shown in Figure 14, with material parameters from Table 1 for the viscosity-dominated regime. We initialize the fully-coupled solver as described in Section 4.1 for a crack of initial length $\bar{\ell} = 6m$. We assume no far field stress on the remote boundary and a critical fracture stress $\sigma_c = 6.0MPa$. The mesh is refined in the neighborhood of the two cracks, where the mesh size is $h = 0.1m$, and the polynomial order of interpolation is $p = 3$, resulting in about 1.6 million degrees of freedom. The constant time-step is $\Delta t = 0.025s$.

Figure 15 shows the time evolution of the solid stress and fluid pressure fields. As fluid is injected in the pressurized crack, opening stress builds up leading to fracture propagation. The pressurized crack merges with the dry

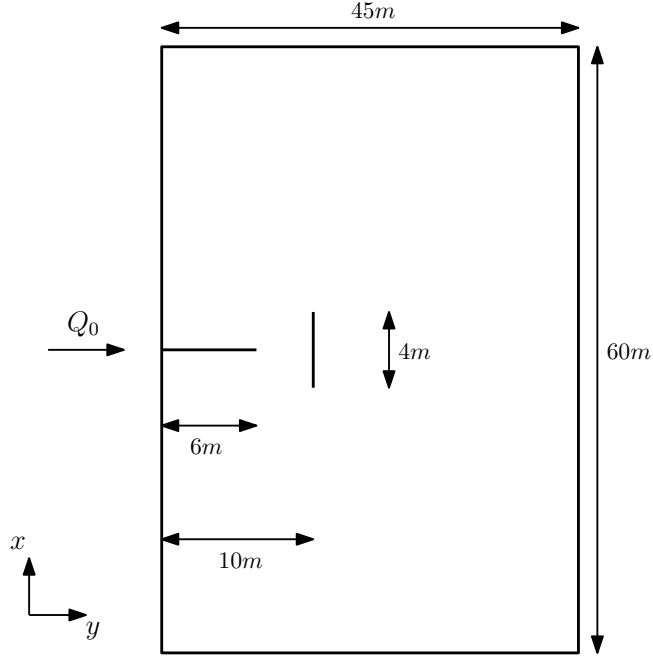


Figure 14: *Schematic of the problem geometry: interaction of a propagating fluid-driven crack of 6 m initial length with a 4 m pre-existing dry crack orthogonal to the fluid-driven crack at a 4 m distance.*

crack, where fluid fills the previously empty space reaching the crack tips. As pressure builds up in the newly activated crack, further crack propagation occurs. It is important to point out that, although the resulting crack path looks qualitatively symmetric, the unstructured character of the mesh leads to actual symmetry breakdown.

This simulation was run in parallel on 256 processors. Figure 16 shows the final state of the calculation, highlighting the seamless propagation of cracks across processor boundaries.

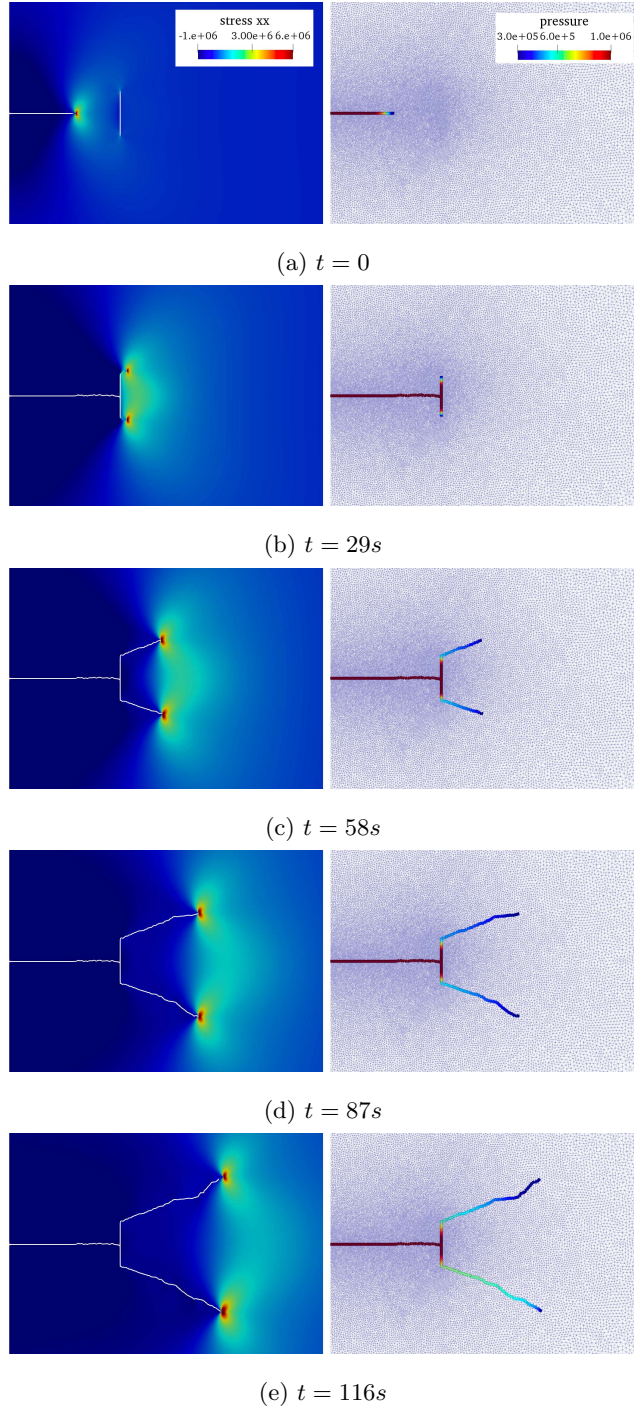


Figure 15: Snapshots of the time evolution of the stress field (left) and fluid pressure field (right). Fluid is injected in the 6 m long initial crack. As opening stress builds up and reaches the critical stress, the crack propagates and merges with the pre-existing dry crack. The fluid fills up previously empty space in the dry crack, applying increasing pressure at the crack lips and leading eventually to further propagation.

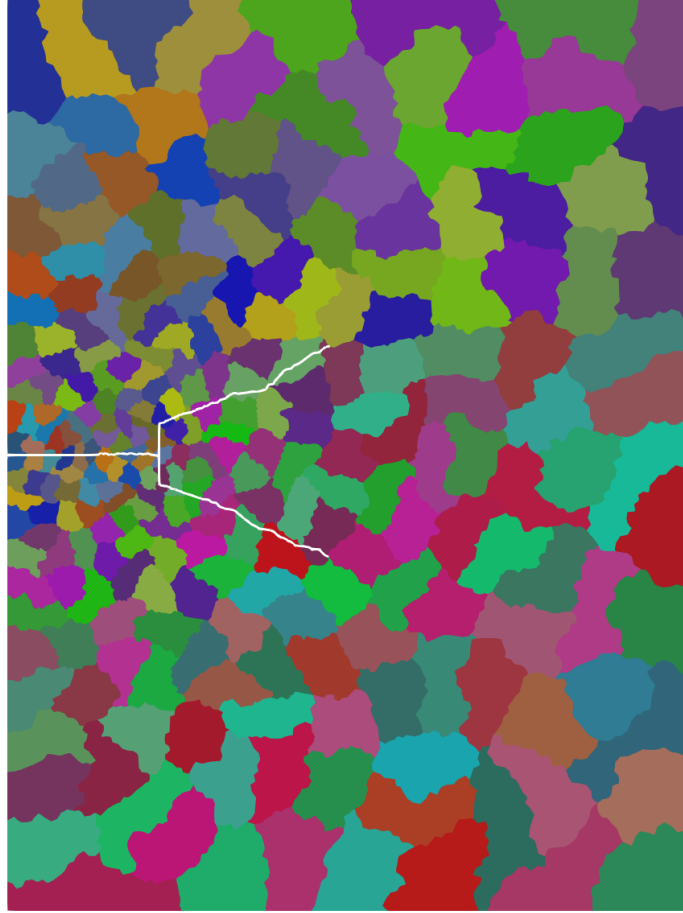


Figure 16: *Final state of a parallel simulation involving a propagating fluid-filled crack interacting with a pre-existing crack and further branching. Each color represents one of the 256 different mesh partitions in the parallel calculation.*

4.6. Assessment of parallel scalability

In order to assess the parallel scalability of the proposed computational framework we performed a strong scaling test on a cluster consisting of 30 nodes, each node having 24 Intel 2.3 GHz Xeon E5-2670 64-bit processors with 62.8 GB memory. In Figure 17 we report the wall time required to perform one time step of the benchmark presented in Section 4.2 (typically consisting of 5-10 iterations of the nonlinear solver), for four different problem sizes (455,000, 1,800,000, 7,200,000, and 29,000,000 degrees of freedom in the fully-coupled system of equations) and for a number of processor ranging from 4 to 700. Figure 17 shows that in the proposed framework parallel computations can lead to a significant reduction in the simulation time, *e.g.* the computation time per time step can be reduced from 53 minutes to 47 seconds by employing 256 processors instead of 4 for a problem size of 1.8 million degrees of freedom, and from 57 to 22 minutes by employing 700 processors instead of 350 for a problem size of 29 million degrees of freedom. Possible sources of parallel inefficiencies include the slight imbalance of workload among processors due to the inactive degrees of freedom in the fluid domain of most of the processors.

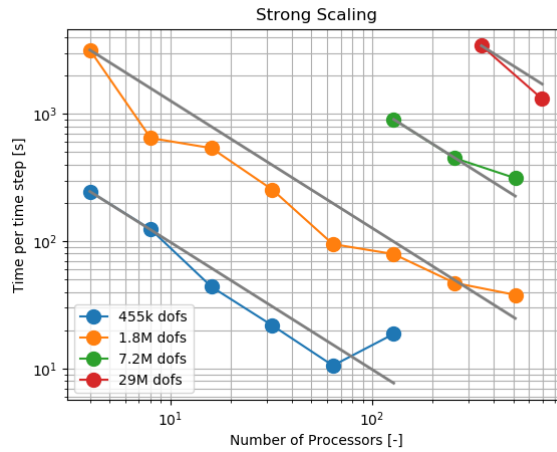


Figure 17: *Strong scaling analysis of the wall time per time step against the number of processors employed in the parallel calculation.*

5. Conclusions

We presented a computational framework to simulate fluid-driven fracture propagation in impermeable solids, addressing the issue of enabling propagation of cracks with arbitrarily intricate paths in a suitable framework for parallel large-scale simulations.

We adopted a hybrid approach in which the solid is described within the DG/CZM framework [26], which facilitates the description of crack propagation, coupled with standard lubrication interface finite elements placed on all mesh interfaces, where fluid flow is activated in newly created channels. We solved the discretized fully-coupled nonlinear system with a conventional Newton-Raphson procedure, which we found robust, provided that the fluid domain is kept fixed during the nonlinear iterations and updated only upon convergence. We showed that a *fully-coupled* treatment of the solid and fluid problems is essential, as a *staggered* solution strategy suffers from both ill-posedness and convergence issues, as it hides the nonlinearity, which appears only in the fluid-solid coupling.

We extensively verified the proposed framework in simplified configurations that admit analytical solutions, namely in the cases of plane strain and penny-shaped cracks. We also showed that the method is able to describe intricate crack paths, including crack branching and merging, in a robust way. We demonstrated that the proposed approach can handle the limitation of constraining the paths to the interelement boundary with a proper mesh resolution, while still retaining the correct description of the fluid equations and the massive scalability, which we have assessed up to 30 million degrees of freedom on a 700 processors distributed memory machine.

References

- [1] B. Lecampion, A. Bungler, X. Zhang, Numerical methods for hydraulic fracture propagation: a review of recent trends, *Journal of Natural Gas*

- Science & Engineering 49 (2017) 66–83. [doi:10.1016/j.jngse.2017.10.012](https://doi.org/10.1016/j.jngse.2017.10.012).
- [2] M. Economides, K. Nolte, Reservoir Stimulation, 3rd Edition, John Wiley & Sons, Chichester, UK, 2000.
 - [3] S. Khristianovich, Y. Zheltov, Formation of vertical fractures by means of highly viscous liquid, in: Proceedings Fourth World Petroleum Congress, Section II/T.O.P., Paper 3, Rome, 1955, pp. 579–586.
 - [4] J. Geertsma, F. de Klerk, A rapid method of predicting width and extent of hydraulically induced fractures, Journal of Petroleum Technology 21 (12) (1969) 1571–1581. [doi:10.2118/2458-PA](https://doi.org/10.2118/2458-PA).
 - [5] J. I. Adachi, Fluid-driven fracture in permeable rock, Ph.D. thesis, University of Minnesota (2001).
 - [6] J. I. Adachi, E. Detournay, Self-similar solution of a plane-strain fracture driven by a power-law fluid, International Journal for Numerical and Analytical Methods in Geomechanics 26 (6) (2002) 579–604. [doi:10.1002/nag.213](https://doi.org/10.1002/nag.213).
 - [7] E. Detournay, [Propagation regimes of fluid-driven fractures in impermeable rocks](#), International Journal of Geomechanics 4 (2004) 35–45. [doi:10.1061/\(ASCE\)1532-3641\(2004\)4:1\(35\)](https://doi.org/10.1061/(ASCE)1532-3641(2004)4:1(35)).
 - [8] D. Garagash, E. Detournay, Plane-strain propagation of a fluid-driven fracture: Small toughness solution, Journal of Applied Mechanics 72 (6) (2005) 916–928. [doi:10.1115/1.2047596](https://doi.org/10.1115/1.2047596).
 - [9] A. P. Bunger, E. Detournay, D. I. Garagash, [Toughness-dominated hydraulic fracture with leak-off](#), International Journal of Fracture 134 (2005) 175–190. [doi:10.1007/s10704-005-0154-0](https://doi.org/10.1007/s10704-005-0154-0).
 - [10] J. I. Adachi, E. Detournay, Plane strain propagation of a hydraulic fracture in a permeable rock, Engineering Fracture Mechanics 75 (16) (2008) 4666–4694. [doi:10.1016/j.engfracmech.2008.04.006](https://doi.org/10.1016/j.engfracmech.2008.04.006).

- [11] T. Boone, A. Ingraffea, [A numerical procedure for simulation of hydraulically-driven fracture propagation in poroelastic media](#), International Journal for Numerical and Analytical Methods in Geomechanics 14 (1990) 27–47. [doi:10.1002/nag.1610140103](#).
- [12] B. Carrier, S. Granet, [Numerical modeling of hydraulic fracture problem in permeable medium using cohesive zone model](#), Engineering Fracture Mechanics 79 (2012) 312–328. [doi:10.1016/j.engfracmech.2011.11.012](#).
- [13] R. R. Settigast, P. Fu, S. D. C. Walsh, J. A. White, C. Annavarapu, F. J. Ryerson, [A fully coupled method for massively parallel simulation of hydraulically driven fractures in 3-dimensions](#), International Journal for Numerical and Analytical Methods in Geomechanics 41 (2017) 627–653. [doi:10.1002/nag.2557](#).
- [14] Z. Chen, A. P. Bunger, X. Zhang, R. G. Jeffrey, [Cohesive zone finite element-based modeling of hydraulic fractures](#), Acta Mechanica Sinica Sinica 22 (2009) 443–452. [doi:10.1016/S0894-9166\(09\)60295-0](#).
- [15] E. Sarris, P. Papanastasiou, [The influence of the cohesive process zone in hydraulic fracturing modelling](#), International Journal of Fracture 167 (2011) 33–45. [doi:10.1007/s10704-010-9515-4](#).
- [16] M. J. Hunsweck, Y. Shen, A. J. Lew, A finite element approach to the simulation of hydraulic fractures with lag, International Journal for Numerical and Analytical Methods in Geomechanics 37 (9) (2013) 993–1015. [doi:10.1002/nag](#).
- [17] T. Belytschko, T. Black, Elastic crack growth in finite element with minimal remeshing, International Journal for Numerical Methods in Engineering 45 (5) (1999) 601–620. [doi:10.1002/\(SICI\)1097-0207\(19990620\)45:5<601::AID-NME598>3.0.CO;2-S](#).
- [18] N. Moës, J. Dolbow, T. Belytschko, [A finite element method for crack](#)

- growth without remeshing, International Journal for Numerical Methods in Engineering 46 (1999) 131–150.
- [19] A. R. Khoei, M. Hirmand, M. Vahab, M. Bazargan, [An enriched fem technique for modeling hydraulically driven cohesive fracture propagation in impermeable media with frictional natural faults: Numerical and experimental investigations](#), International Journal for Numerical Methods in Engineering 104 (2015) 439–468. doi:[10.1002/nme.4944](#).
 - [20] T. Mohammadnejad, J. E. Andrade, [Numerical modeling of hydraulic fracture propagation, closure and reopening using xfem with application to in-situ stress estimation](#), International Journal for Numerical and Analytical Methods in Geomechanics 40 (2016) 2033–2060. doi:[10.1002/nag.2512](#).
 - [21] E. Gordeliy, A. Peirce, [Coupling schemes for modeling hydraulic fracture propagation using the xfem](#), Computer Methods in Applied Mechanics and Engineering 253 (2013) 305–322. doi:[10.1016/j.cma.2012.08.017](#).
 - [22] P. Gupta, C. A. Duarte, [Simulation of non-planar three-dimensional hydraulic fracture propagation](#), International Journal for Numerical and Analytical Methods in Geomechanics 38 (2014) 1397–1430. doi:[10.1002/nag](#).
 - [23] P. Gupta, C. A. Duarte, Coupled formulation and algorithms for the simulation of non-planar three-dimensional hydraulic fractures using the generalized finite element method, International Journal for Numerical and Analytical Methods in Geomechanics 40 (2016) 1402–1437. doi:[10.1002/nag.2485](#).
 - [24] P. Gupta, C. A. Duarte, Coupled hydromechanical-fracture simulations of nonplanar three-dimensional hydraulic fracture propagation, International Journal for Numerical and Analytical Methods in Geomechanics 42 (1) (2018) 143–180. doi:[10.1002/nag.2719](#).
 - [25] B. L. Karihaloo, Q. Z. Xiao, Modelling of stationary and growing cracks in FE framework without remeshing: A state-of-the-art review, Comput-

- ers and Structures 81 (3) (2003) 119–129. [doi:10.1016/S0045-7949\(02\)00431-5](#).
- [26] R. Radovitzky, A. Seagraves, M. Tupek, L. Noels, A scalable 3D fracture and fragmentation algorithm based on a hybrid, discontinuous Galerkin, Cohesive Element Method, *Computer Methods in Applied Mechanics and Engineering* 200 (2011) 326–344. [doi:10.1016/j.cma.2010.08.014](#).
- [27] G. A. Francfort, J.-J. Marigo, Revisiting brittle fracture as an energy minimization problem, *Journal of the Mechanics and Physics of Solids* 46 (1998) 1319–1342. [doi:10.1016/S0022-5096\(98\)00034-9](#).
- [28] B. Bourdin, G. A. Francfort, J.-J. Marigo, Numerical experiments in revisited brittle fracture, *Journal of the Mechanics and Physics of Solids* 48 (4) (2000) 797–826. [doi:10.1016/S0022-5096\(99\)00028-9](#).
- [29] B. Bourdin, The variational formulation of brittle fracture: numerical implementation and extensions, *IUTAM Symposium on Discretization Methods for Evolving Discontinuities* (2007) 381–393.
- [30] M. F. Wheeler, T. Wick, W. Wollner, [An augmented-lagrangian method for the phase-field approach for pressurized fractures](#), *Computer Methods in Applied Mechanics and Engineering* 271 (2014) 69–85. [doi:10.1016/j.cma.2013.12.005](#).
- [31] C. V. Verhoosel, R. de Borst, A phase-field model for cohesive fracture, *International Journal for Numerical Methods in Engineering* 96 (2013) 43–62. [doi:10.1002/nme.4553](#).
- [32] Z. Wilson, C. Landis, Phase-field modeling of hydraulic fracture, *Journal of the Mechanics and Physics of Solids* 96 (2016) 264–290. [doi:10.1016/j.jmps.2016.07.019](#).
- [33] C. Miehe, S. Mauthe, Phase field modeling of fracture in multi-physics problems. Part III. Crack driving forces in hydro-poro-elasticity and hydraulic fracturing of fluid-saturated porous media, *Computer Methods in*

- Applied Mechanics and Engineering 304 (2015) 619–655. [doi:10.1016/j.cma.2015.09.021](#).
- [34] S. Lee, A. Mikelić, M. F. Wheeler, T. Wick, Phase-field modeling of proppant-filled fractures in a poroelastic medium, Computer Methods in Applied Mechanics and Engineering 312 (2016) 509–541. [doi:10.1016/j.cma.2016.02.008](#).
- [35] B. Giovanardi, A. Scotti, L. Formaggia, [A hybrid xfem -phase field \(xfield\) method for crack propagation in brittle elastic materials](#), Computer Methods in Applied Mechanics and Engineering 320 (2017) 396–420. [doi:10.1016/j.cma.2017.03.039](#).
- [36] A. Seagraves, R. Radovitzky, Large-scale 3D modeling of projectile impact damage in brittle plates, Journal of the Mechanics and Physics of Solids 83 (2015) 48–71. [doi:10.1016/j.jmps.2015.06.001](#).
- [37] S. A. Serebrinsky, M. Sánchez, D. Smilovich, R. Toscano, A. Rosolen, M. B. Goldschmit, E. N. Dvorkin, R. Radovitzky, Desarrollo y Validación de un Simulador de Fracturamiento Hidráulico Orientado al Petróleo y Gas, in: Congreso sobre Métodos Numéricos y sus Aplicaciones, Vol. XXXIV, 2016, pp. 8–11.
- [38] M. Hirmand, M. Vahab, K. Papoulia, N. Khalili, Robust simulation of dynamic fluid-driven fracture in naturally fractured impermeable media, Computer Methods in Applied Mechanics and Engineering 357 (2019) 112574. [doi:10.1016/j.cma.2019.112574](#).
- [39] M. Vahab, N. Khalili, Computational algorithm for the anticipation of the fluid-lag zone in hydraulic fracturing treatments, International Journal of Geomechanics 18 (10) (2018) 1–15. [doi:10.1061/\(ASCE\)GM.1943-5622.0001273](#).
- [40] G. Howard, C. R. Fast, [Optimum fluid characteristics for fracture extension](#), Proceedings of the American Petroleum Institute (1957) 261–270.

- [41] B. Giovanardi, L. Formaggia, A. Scotti, P. Zunino, [Unfitted fem for modelling the interaction of multiple fractures in a poroelastic medium](#), Lecture Notes in Computational Science and Engineering 121. [doi:10.13140/RG.2.2.33012.35207](#).
- [42] G. Barenblatt, [The mathematical theory of equilibrium cracks in brittle fracture](#), Advances in Applied Mechanics 7 (1962) 55–129. [doi:10.1016/S0065-2156\(08\)70121-2](#).
- [43] G. I. Barenblatt, [The formation of equilibrium cracks during brittle fracture. general ideas and hypotheses. axially-symmetric cracks.](#), Journal of Applied Mathematics and Mechanics 23 (3) (1959) 622–636.
- [44] G. Camacho, M. Ortiz, [Computational modeling of impact damage in brittle materials](#), International Journal of Solids and Structures 33 (20–22) (1996) 2899–2983. [doi:10.1016/0020-7683\(95\)00255-3](#).
- [45] L. Noels, R. Radovitzky, A general discontinuous Galerkin method for finite hyperelasticity. Formulation and numerical applications, International Journal for Numerical Methods in Engineering 68 (1) (2006) 64–97. [doi:10.1002/nme.1699](#).
- [46] L. Noels, R. Radovitzky, An explicit discontinuous Galerkin method for non-linear solid dynamics. Formulation, parallel implementation and scalability properties., International Journal for Numerical Methods in Engineering 74 (9) (2007) 1393–1420. [doi:10.1002/nme.2213](#).
- [47] G. Karypis, V. Kumar, MeTis: Unstructured Graph Partitioning and Sparse Matrix Ordering System, Version 4.0, <http://www.cs.umn.edu/~metis> (2009).
- [48] S. Balay, J. Brown, P. Brune, K. Buschelman, L. Dalcin, V. Eijkhout, W. Gropp, D. Karpeyev, D. Kaushik, M. Knepley, L. C. McInnes, B. Smith, S. Zampini, H. Zhang, Petsc users manual, Tech. Rep. ANL-95/11 - Revision 3.7, Argonne National Laboratory (2016).

- [49] B. Lecampion, E. Detournay, An implicit algorithm for the propagation of a hydraulic fracture with a fluid lag, *Computer Methods in Applied Mechanics and Engineering* 196 (2007) 4863–4880. doi:[10.1016/j.cma.2007.06.011](https://doi.org/10.1016/j.cma.2007.06.011).
- [50] D. I. Garagash, E. Detournay, The Tip Region of a Fluid-Driven Fracture in an Elastic Medium, *Journal of Applied Mechanics* 67 (1) (1999) 183–192. doi:[10.1115/1.321162](https://doi.org/10.1115/1.321162).
- [51] D. I. Garagash, Propagation of a plane-strain hydraulic fracture with a fluid lag: Early-time solution, *International Journal of Solids and Structures* 43 (18-19) (2006) 5811–5835. doi:[10.1016/j.ijsolstr.2005.10.009](https://doi.org/10.1016/j.ijsolstr.2005.10.009).
- [52] D. I. Garagash, Cohesive-Zone Effects in Hydraulic Fracture Propagation, *Journal of the Mechanics and Physics of Solids* (2019) 103727doi:[10.1016/j.jmps.2019.103727](https://doi.org/10.1016/j.jmps.2019.103727).
- [53] E. Detournay, Propagation regimes of fluid-driven fractures in impermeable rocks, *International Journal of Geomechanics* 4 (1) (2004) 35–45. doi:[10.1061/\(ASCE\)1532-3641\(2004\)4:1\(35\)](https://doi.org/10.1061/(ASCE)1532-3641(2004)4:1(35)).
- [54] G. Irwin, Analysis of stresses and strains near the end of a crack traversing a plate, *Journal of Applied Mechanics* 24 (1957) 361–364.
- [55] D. Garagash, Hydraulic fracture propagation in elastic rock with large toughness, in: *Proc. 4th North American Rock Mechanics Symp.*, 2000, pp. 221–228.
- [56] A. Savitski, E. Detournay, Propagation of a penny-shape hydraulic fracture in an impermeable rock, *International Journal of Solids and Structures* 39 (2002) 6311–6337. doi:[http://dx.doi.org/10.1016/S0020-7683\(02\)00492-4](http://dx.doi.org/10.1016/S0020-7683(02)00492-4).
- [57] D. Chuprakov, O. Melchaeva, R. Prioul, Hydraulic Fracture Propagation Across a Weak Discontinuity Controlled by Fluid Injection, in: *Effective*

and Sustainable Hydraulic Fracturing, IntechOpen, 2013, Ch. 8. doi:<http://dx.doi.org/10.5772/57353>.